HEMPT Downscaling, Way Forward to the First EM for CubeSat Applications

IEPC-2017-274

Presented at the 35th International Electric Propulsion Conference
Georgia Institute of Technology – Atlanta, Georgia – USA
October 8–12, 2017

Franz Georg Hey*and Max Vaupel†
Airbus, Friedrichshafen, Germany

Claus Braxmaier
DLR, Institute of Space Systems, Bremen, Germany
Universität Bremen, ZARM, Bremen, Germany

Martin Tajmar
Technische Universität Dresden, Institute of Aerospace Engineering, Dresden, Germany

and

Alexander Sell, Karlheinz Eckert, Dennis Weise, Noah Saks, and Ulrich Johann
Airbus, Friedrichshafen, Germany

Airbus downscales a High Efficiency Multistage Plasma Thruster (HEMPT) or cusped field thruster down to the micro-Newton regime. This thruster could also be used for CubeSat missions in order to enable orbit manoeuvring such as orbit raising. Currently, several three unit CubeSats are in development which could provide enough payload power to operate a small electric thruster on-board.

Based on the experience gained, we decided to start the development of a propulsion system which is especially designed for CubeSat applications based on our HEMPT or cusped field thruster technology.

As a first step, an engineering model of the propulsion system has been developed which consists of a thruster, a thermionic cathode and a COTS power converter. This thruster system has successfully been built and characterised.

The first measurement results are presented and an outlook of the further development steps will be given.

*Technical Lead, Laboratory for Enabling Technologies, franz.hey@airbus.com
†PhD student, Laboratory for Enabling Technologies, max.vaupel@airbus.com

Nomenclature

GAIA	= Global Astrometric Interferometer for Astrophysics
LISA	= Laser Interferometer Space Antenna
AOCS	= Attitude and Orbit Control System
FEEP	= Field Electric Emission Propulsion
RIT	= Radio Frequency Ion Thruster
HEMPT	= High Efficiency Multistage Plasma Thruster
COTS	= Commercial Off the Shelf
OLV	= Oerlikon Leybold Vacuum
ESC	= Electro-Static Comb
PSD	= Power Spectral Density

I. Introduction

In 2009 Airbus in Friedrichshafen started to downscale a High Efficiency Multistage Plasma Thruster (HEMPT) sometimes called cusped field thruster to micro-Newton thrust levels. The motivation behind this activity was twofold, firstly to create in-house hands-on experience with electric propulsion, especially to better understand the challenges electric propulsion for highly precise AOCS faces and secondly to experimentally demonstrate that the cusped field thruster principle can be used within micro-Newton thrust levels.

In figure 1, the HEMPT or cusped field principle is illustrated. The cylindrical discharge channel is surrounded by three magnetic rings, forming three cusps inside the discharge channel. At the thruster exit an electron source emits electrons to neutralise the extracted ion beam and to maintain the plasma discharge. The electrons are confined inside the cusped field structured magnetic field topology. These electrons can collide with neutral particles of the propellant that are fed into the discharge chamber through the anode. This electron bombardment is ionising the propellant and the ionised particles are accelerated in the electric field between anode and cathode. Therefore, the thruster principle offers high specific impulses of an electric thruster paired with a reduced system complexity.

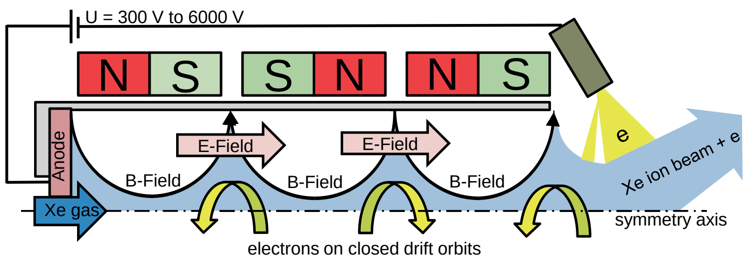

Figure 1. Schematic view of the HEMPT concept. The cylindrical discharge channel is surrounded by three magnetic rings, forming three cusps inside the discharge channel. At the thruster exit an electron source emits electrons to neutralise the extracted ion beam and to maintain the plasma discharge. The electrons are confined inside the cusp field structured magnetic field topology.

The thruster down-scaling has been performed via a semi-empirical development approach, i.e. numerical magnetic field simulations and particle tracing has been combined with a qualitative model of the thruster and extensive experimental thruster testing campaigns. The preliminary results of these campaigns has been presented at the IEPC 2013 and 2015 [1, 2].

One result of this development approach is a magnetic field configuration of the thruster which is strongly modified with respect to the originally published HEMPT concept as it is shown in figure 1. Internally, this magnetic field configuration is called Advanced Cusped Field Thruster (ACFT). The downscaling has been continued based on this field configuration.

In parallel to the optimisation of the magnet field itself, also other developments are required in order to efficiently operate a cusped field thruster at micro-Newton thrust levels. A major loss mechanism, caused by downscaling, is the electron loss at the discharge chamber wall due to the fact that the maximum magnetic field strength is limited by the permanent magnets used and cannot be increased significantly. Therefore, the Lamor radii of the electrons inside the discharge chamber are kept constant which leads to an increase loss of electrons if the discharge chamber dimensions are reduced. This is required in order to maintain a sufficient neutral gas background pressure in the chamber to maintain the plasma discharge. In addition this effect is amplified because of the involved materials and processes. In particular, the discharge chamber wall thickness can not be linearly reduced because of the ceramic machining involved.

Thus, a major improvement was the replacement of the solid ceramic discharge chamber by a ceramic coating which has been directly deposited onto the magnet stack. The principle is illustrated in figure 2, where the qualitatively thruster dimensions, with a machined ceramic chamber on the left side and a coated chamber on the right side, are compared. The ceramic discharge chamber coating enables a minimal thickness of the chamber walls. Therefore, electron losses at the chamber wall are minimal. Consequently, the thruster efficiently operates despite its smaller dimensions.

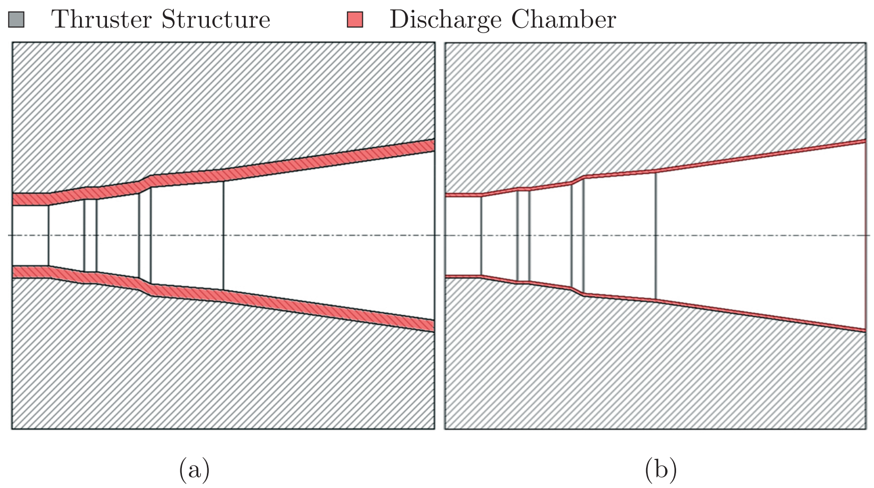

Figure 2. Illustration between a conventionally manufactured discharge chamber (left side) and the coated discharge chamber. The coating enables a minimal wall thickness. Hence, the electron losses inside the discharge chamber are reduced.

II. Three Unit CubeSat Thruster

Following the approach described, a thruster has been designed which is capable to be efficiently operated in the micro-Newton regime [3]. It has been identified that the thruster could be used as main thruster on a CubeSat mission. A preliminary analysis with the System Design Toolkit has demonstrated that the thruster would allow to perform orbit raising of several hundreds of kilometres with a CubeSat. The final system shall consists of a thruster, a cathode, a DC/DC converter as simple power processing unit and a propellant feeding infrastructure. As propellant Iodine shall be used.

Therefore, the thruster has been further developed as potential main thruster of a three unit Cubesat. As a first step, a thruster system Engineering Model (EM) has been built. The thruster system has been designed to have a maximum input power of up to 10 W and therefore up to 200 µN thrust. Currently, 200 µN cannot be achieved due to the maximum output current of 6 mA of the commercial of the shelf DC/DC converter used. Figure 3 shows photographs of the thruster system. In a) the complete system is presented. The thruster itself is shown in the middle. The discharge chamber diameter is 7 mm wide. At the upper side the thermionic cathode used can be seen.

The thruster system is designed to fit in 1/2 unit plus a Tunacan extension. In the inside of the housing, a Commercial Of the Shelf (COTS) DC/DC converter is placed as well which is required to operate the thruster. The actual EM did not include the propellant feed architecture. However, the housing offers sufficient space in order to accommodate all required equipment. For the thruster itself, a thermal analysis has been already performed. With respect to the outcome of this analysis, the Tunacan part of the housing has been used as radiator.

The firing thruster is presented in figure 3 b). The thruster has been exclusively fired with Xenon so far. The figure illustrates the characteristic xenon discharge. Above the thruster the thermionic cathode is visible. Currently, the hot cathode is made of tungsten, i.e. the cathode has to be heated up to more than 2000 K in order to emit a sufficient electron current. The bright shine of the cathode illustrates the high temperature. The final design shall incorporate a thermionic cathode made of Lanthanum Hexaborid. This is required in order to reduce the necessary cathode heating power to a minimum for optimising the system Power To Thrust Ratio (PTTR). Additionally, it is planed to replace the COTS converter in order to overcome this limitation and to increase the converter efficiency.

A mapping of the plume of the thruster is presented in figure 4 where the normalised current density is plotted versus the planar angle. The current density of each curve was normalised to the maximum measured current density which was measured in each data set. The measurements have been performed at a constant

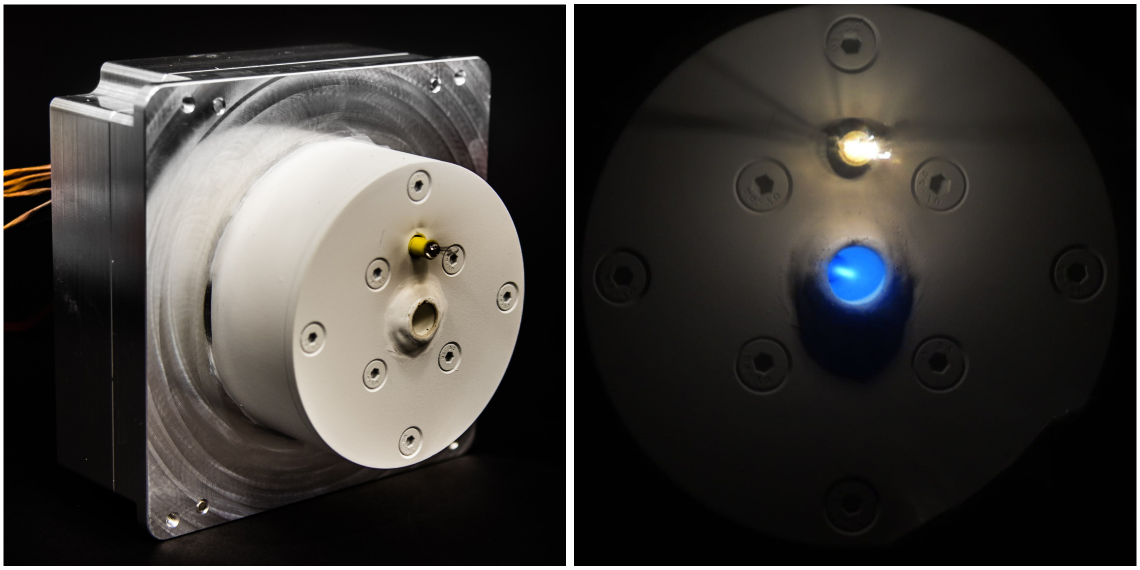

(a) (b)

Figure 3. Images of the CubeSat thruster system developed. In a) the thruster is shown, fitting in a 1/2 unit plus Tunacan housing. In b) the thruster firing is shown. Its thermionic cathode can be seen as bright light above the xenon discharge.

propellant mass flow of 0.1 sccm. In all curves, the measured beam current density at angular positions larger 80 degree is zero or almost zero. This is the result of the thruster structure which blocks the ion beam at angles greater than 80 degree.

The figure enables a comparison of the plume shape at different anode potential levels. In purple, the measured angular current density distribution at 441 V anode potential and 6 mA anode current is presented. The processing of the measured data leads to a divergence efficiency of $\gamma = 60\,\%$ and a discharge efficiency of $\eta_d = 60\,\%$. In the centre of the plume a current density gap can be seen. The plume has a qualitatively shape which is comparable to an advanced cusped field thruster with a wider discharge chamber diameter as it is presented in [4].

The green curve presents the measurement result at 811 V anode potential and 5.4 mA anode current. The plume is more focused to the rotation axis which results in an increased divergence efficiency of $\gamma = 70\,\%$. Moreover, the discharge efficiency is $\eta_d = 91\,\%$ i.e. it is also increased.

The red curve in figure 4 illustrates the shape of the plume at an anode potential of 1504 V and an anode current of 2.75 mA. It can be seen that the current density in the centre of the plume is increased compared to the lower potentials. The gap that can be observed at 441 V and 811 V is not visible any more. Therefore, the divergence efficiency is slightly higher than at lower anode potential levels. Although the beam has a more Gaussian shape, the increase of the divergence efficiency is comparably small, this is a result of the qualitatively high amount of current density at higher angular positions. In contrast to the increased divergence efficiency, the discharge efficiency is reduced to 53 %. Therefore, the total efficiency at this operation point is slightly lower as at the 811 V operation point.

The figure illustrates that although the magnetic field has been optimised for small thruster dimensions, the influence of the magnetic field on the plasma plume is reduced especially in comparison with a comparable thruster as it is presented in [4]. Moreover, the plot illustrates that the overall operational flexibility is also being reduced and that it is essential to operate the thruster at an sufficient operation point in order to achieve an adequate performance.

All tested operation points are presented in figure 5, where the specific impulse is plotted versus the mass flow. Each tested point is marked by a red cross. Next to the crosses, the measured operation parameters are written. The first value is the directly measured absolute thrust, the second value is the anode potential and the third parameter is the anode current. The directly measured thrust has been used to calculate the specific impulse and the total efficiency of the thruster. It is in the range of 3 % to 7 %.

The minimal mass flow that has been used for detailed testing was 0.1 sccm. Even at this mass flow level

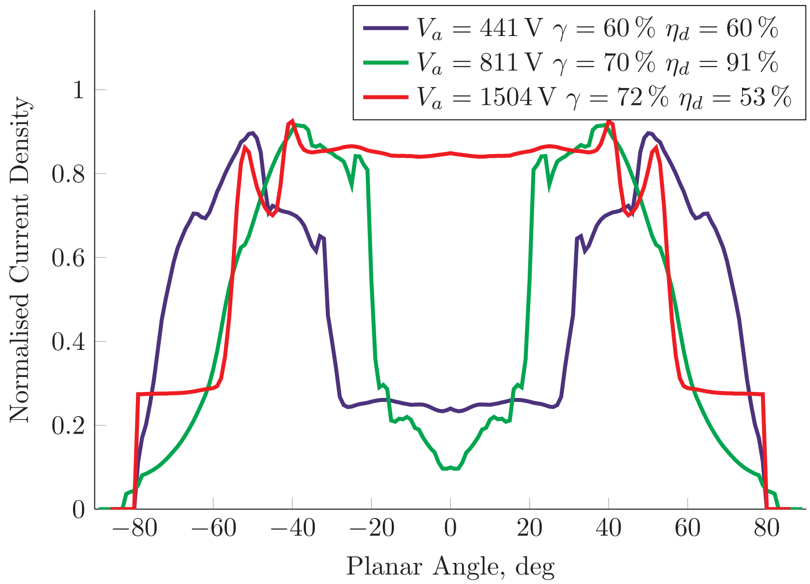

Figure 4. The curves illustrate the plume shapes of the developed thruster at different anode voltage levels at a constant propellant mass flow of 0.1 sccm. The anode current differs for various operation points, thus the current density is normalised to maximal measured current density of each operation poin in this plot. It is plotted versus the planar angle position in degrees. The curves illustrate that the shape of the plume and therefore the divergence efficiency is strongly dependent on the anode voltage.

the thruster operated stable. Hence, detailed measurements could be performed. Directly at 0.1 sccm, the thruster could be operated in a range between 29 µN and 86 µN. The thruster could be mainly throttled by the variation of the anode voltage. At higher anode voltages also the anode currents increased.

At the flow rate of 0.1 sccm, the operation point with the highest specific impulse was measured at 86 µN with an anode voltage of 1300 V, an anode current of 5.8 mA and a total efficiency of 5.5 %.

At 0.2 sccm propellant mass flow, different tests has been performed as well. It was possible to operate the thruster at different anode potentials and anode current levels. At higher mass flows, the thruster could be operated, but the maximum anode current was limited by the DC/DC converter used, limiting the overall thruster performance at higher propellant feeding rates.

As part of the thruster system characterisation campaign, also thrust noise measurements have been performed. For the thrust noise measurements, a FUG laboratory power supply and a Bronkhorst laboratory Xenon mass flow controller have been used.

The result of the measurement is presented in figure 6, where the thrust noise is plotted versus the frequency. The shown PSDs are derived from a 20 h measurement which has been down-sampled to 20 Hz. A Blackman-Harris 92 window has been used to generate the curves.

The measurement has been performed at an anode potential of 670 V with an anode current of 4.2 mA. The mass flow was used to control the thrust. Thus, a digital PI-controller has been implemented to stabilise the anode current at the mentioned level of 4.2 mA. Due to the long tube distance between the mass flow controller and the thruster, the transient time of the control loop was long. Hence, the controller was not able to control short term anode current fluctuations. For a correct understanding of the curves that are presented in the following, it is important to mention that the direct thrust noise measurement includes all potential noise sources within the thruster system.

In Figure 6, the blue curve illustrates the thrust noise requirement of NGGM and Euclid. The black curve presents the thrust noise requirement of LISA.

The PSD that is shown as yellow curve represents the result of the direct thrust noise measurement of the miniaturised system.

Between 1 Hz and $81 \cdot 10^{-2}$ Hz the measured thrust noise is below 0.1 µN. At lower frequencies the thrust noise increases to 1 µN. At frequencies lower than $1 \cdot 10^{-3}$ Hz pink noise starts to dominate the measured thrust noise.

Hence, the tested thruster fulfils the LISA requirement at frequencies between 1 Hz and $8 \cdot 10^{-2}$ Hz.

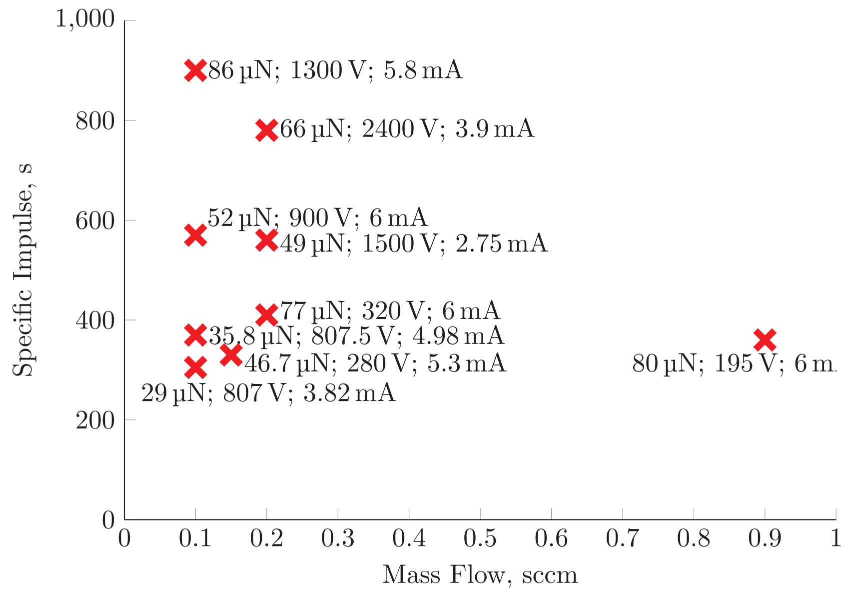

Figure 5. Summary of the tested operation points, where the specific impulse is plotted versus the mass flow. The thruster can be operated over a wide range. The operation point with the smallest achievable measured thrust is 29 µN, with a low I_{sp} of only 295 s. At higher thrust levels, Isps of more than 900 s can be demonstrated.

Beyond this frequencies, the thruster is not compliant with this requirement.

However, the thruster system fulfils the thrust noise requirement of NGGM and Euclid over the whole measurement bandwidth.

In order to compare the directly measured thrust noise performance with the indirect measured thrust noise, also called calculated thrust noise performance, the thrust noise that has been derived from the parallel measured mass flow, anode potential and anode current are presented in figure 6 as red curve.

It can been seen that between 1 Hz and $3 \cdot 10^{-2}$ Hz, the calculated thrust noise level is higher than the directly measured thrust noise level. Between $3 \cdot 10^{-2}$ Hz to $1 \cdot 10^{-3}$ Hz the thrust noise level is equal. After $1 \cdot 10^{-3}$ Hz the calculated thrust noise level remains constant whereas the directly measured thrust noise level starts to rise.

It can be assumed that one reason for the higher calculated thrust noise level is the long propellant feeding line that acts as a low pass filter which is not considered in the calculations. The measured noise of the mass flow might exceed the real noise of the mass flow at the thruster. The curves illustrate that this difference falsifies the indirect thrust noise measurement.

In order to avoid this, a thrust noise estimation which is exclusively based on the measured anode potential and the anode current has been performed as well. It is presented as green curve. As expected, the thrust noise level is reduced in comparison to the previous calculation. But, the thrust noise level between 1 Hz and $3 \cdot 10^{-2}$ Hz is still higher than the directly measured thrust noise (yellow curve). Thus, the measured anode current noise must be higher than the real noise of the ion beam.

The results underline that the thrust noise calculation via the simple assessment of the anode potential and the anode current is not sufficient to estimate the real thrust noise performance for the tested thruster. Dependent on the measurement principle and the measurement positions of the anode current, anode potential and propellant mass flow, the indirect thrust noise measurement could generate invalid measurement result. Whereas, the direct thrust noise measurement is able to characterise the complete thruster system.

III. Conclusion

The downscaling of a high efficiency multistage plasma thruster or cusped field thruster by Airbus in Friedrichshafen has been continued and the result has been presented.

The further development is now based on the so-called advanced cusped field thruster magnetic field geometry. The thruster could be used as main thruster of a three unit CubeSat. Therefore, an Engineering

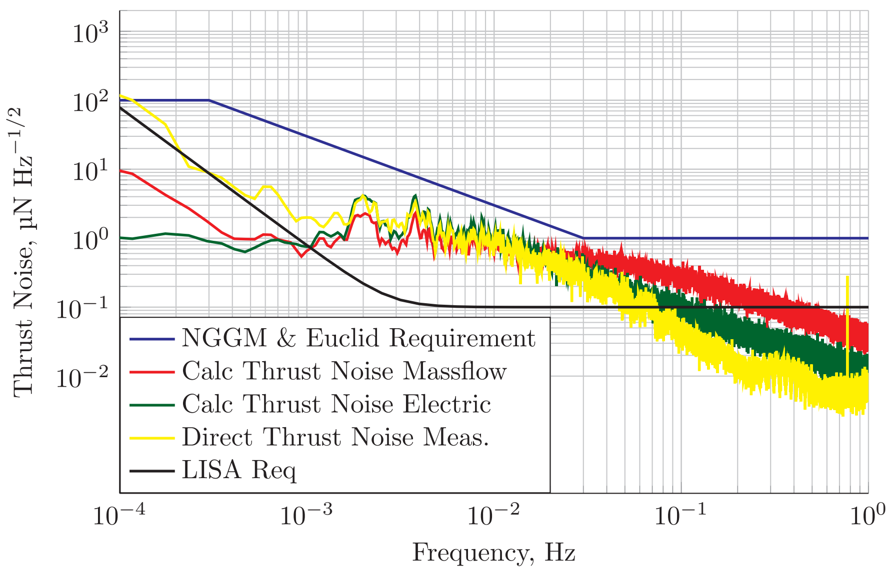

Figure 6. The curve presents a direct thrust noise measurement of the miniaturised thruster in comparison with the targeted requirements and two different indirect estimated noise figures.

Model (EM) has been built to experimentally demonstrate this capability. The design of the EM has been presented. It consists of the thruster itself, a thermionic cathode and a commercial of the shelf high voltage DC/DC converter. The design is generally made to create 200 µN thrust out of 10 W of input power. This has not been demonstrated so far due to the limited output current of the DC/DC converter used.

An overview of the most important results of the measurement campaign has been provided. In table 1 an overview of one of the demonstrated operation points is presented. It can been seen that the total efficiency of the thruster has been increased to more than 5 % and a specific impulse of more than 900 s has been measured. It is expected that, with a power supply that can provide larger output currents, also the absolute thrust can be increased further.

Table 1. Illustration of the parameters of one single point of operation that could be estimated via the direct thrust measurement. This parameters were measured for all operation point.

Parameter	**Value**
Anode voltage	1300 V
Anode current	5.8 mA
Mass flow	0.1 sccm
Thrust	86 µN
I_{sp}	897 s
PTTR	87.7 W/mN
η_T	5.5 %

As next step, the tungsten made thermionic cathode will be replaced by a version made of Lanthanum Hexaborid in order to increase the overall thruster system efficiency. In parallel, the thruster system shall be tested with Iodine as propellant, using an in-house developed Iodine feeding infrastructure [4] which will be miniaturised in order to be compatible with the 1/2 unit plus Tunacan housing. Moreover, the COTS DC/DC converter will be replaced by a custom designed converter which will be able to provide a larger output current. In parallel, the efficiency of the converter will be increased. This activities will lead to a second EM which will be able to fully experimentally demonstrate on thruster system level, that it can be used as CubeSat main thruster in order to enable CubeSat orbit raising and other manoeuvres.

References

[1] Andreas Keller et al., Parametric Study of HEMP-Thruster, Downscaling to µN Thrust Levels, IEPC-2013-269 (2013).
[2] Franz Georg Hey, et al., Downscaling a HEMPT to micro-Newton Thrust levels: current status and latest results, IEPC-2015-377(2015).
[3] Franz Georg Hey, Development and Test of a Micro-Newton Thruster Test Facility and Micro-Newton HEMPTs, Springer (2017, to be published).
[4] Max Vaupel and Franz Georg Hey, et. al. The Next Generation milli-Newton µHEMPT as Potential Main Thruster for Small Satellites, IEPC-2017-275.